Iran University of Science and Technology

Automotive Science and Engineering

Journal Homepage: ase.iust.ac.ir

ISSN: 2717-2023

Effect of hole shapes and dimensions on the crushing performance of octagonal multi-cell columns

S. Pirmohammad[18] , S. Esmaeili-Marzdashti[1] and E. Vosoghifard[1]

[1] Department of Mechanical Engineering, Faculty of Engineering, University of Mohaghegh Ardabili, Ardabil,179, Iran.

ARTICLE INFO

Article history:
Received : 28 Dec 2019
Accepted: 5 March 2020
Published: 1 March 2021

Keywords:
Thin-walled columns
Crushing capability
Hole shape
Octagonal multi-cell column

A B S T R A C T

Thin-walled columns are frequently employed in vehicle structures to diminish the damages resulting from vehicle collisions. In this research, the effect of hole shapes and dimensions on crushing behavior of octagonal multi-cell columns subjected to longitudinal loading is studied. Rectangular, hexagonal and elliptical holes are assumed on the octagonal multi-cell columns, and crushing parameters (i.e. specific energy absorption SEA and maximum crushing force Fmax) are then obtained by performing numerical analyses in LS-DYNA. The results demonstrate that creation of holes on column walls improve crushing capability significantly, such that creation of rectangular, hexagonal and elliptical holes on the octagonal multi-cell columns increases the value of SEA by 37%, 42% and 39%, respectively in comparison to the plain octagonal column. On the other hand, presence of holes on the octagonal columns results in reduction of Fmax (as a negative crushing indicator).

1. Introduction

Thin-walled columns are frequently employed in the vehicle structures because of outstanding features like crushing capability and lightweight [1]. A huge body of literature exists on the improvement of thin-walled columns to reduce the damages resulting from vehicle collisions. For instance, many cross-sectional configurations such as square [2, 3], circular [4, 5], hexagonal [6, 7] and octagonal [8, 9] columns have been proposed by researchers in the past years to increase crushing capability of thin-walled structures. As such, some of the researchers employed the multi-cell, foam filled and conical columns for the purpose of improving the crushing capacity.

As mentioned above, in addition to single-cell columns, multi-cell columns have been popular research subject in recent years for the researchers. For example, Chen and Wierzbicki

* Corresponding author. Tel.: +98 45 3351 5736; fax: +98 45 3351 2904.

E-mail address: s_pirmohammad@uma.ac.ir

https://doi.org/10.22068/ase.2020.433

[DOI: 10.22068/ase.2020.433]

[10] express that the multi-cell columns have 15% higher crushing capability than the single-cell columns. According to Zhang and Cheng [11], the multi-cell columns exhibit 50-100% higher energy absorption efficiency compared to the foam-filled columns. A large number of cross-sectional shapes for the multi-cell columns have been suggested by researchers. For example, Kim [12] suggested new multi-cell profiles to increase crashworthiness capability of square columns. Zhang *et al.* [13-15], Wu *et al.* [1], Chang *et al.* [16], and Pirmohammad *et al.* [17] investigated crashworthiness behavior of multi-cell square columns. Tran *et al.* [18] and Tran and Baroutaji [19] studied crashworthiness of triangular multi-cell tubes. Tang *et al.* [20] used cylindrical multi-cell columns to improve crushing behavior. Krolak *et al.* [21] and Hong *et al.* [22] investigated crushing behavior of triangular multi-cell columns. Hosseini-Tehrani and Pirmohammad [9] studied crashworthiness behavior of concentric thin-walled columns under both axial and oblique loadings. Pirmohammad and Esmaeili-Marzdashti [23, 24] suggested new designs of multi-cell columns. They assessed crashworthiness capacity of these columns under quasi-static and dynamic axial and oblique loadings. Alavi-Nia and Parsapour [25] made an experimental and numerical investigation on crushing behavior of polygonal multi-cell columns. According to their results, the hexagonal and octagonal multi-cell columns showed the highest crushing capacity. Yuen *et al.* [26] investigated crushing performance of double-cell foam-filled columns in which the circular columns are shown to have better performance than square columns. Sun *et al.* [27] studied crushing behavior of aluminum foam filled columns. Pirmohammad and Ahmadi-Saravani investigated crashworthiness of foam-filled multi-cell columns. Esmaeili-Marzdashti *et al.* [28] studied crashworthiness of S-shaped multi-cell structures. In another study, Esmaeili-Marzdashti *et al.* investigated crashworthiness of octagonal multi-cell S-shaped columns, and showed that the octagonal columns have superior capability for energy absorption purposes.

In this paper, the effect of hole shapes and dimensions on crushing behavior of octagonal multi-cell columns under axial loading is studied. Eight holes having three different shapes are assumed on the walls of the octagonal columns, and the crushing parameters are obtained by performing numerical simulations in LS-DYNA.

2. Geometry and FE features

The octagonal multi-cell columns shown in Fig. 1 are made up of two concentric octagonal tubes, which are connected together by four stiffening plates. The size of inner tube is half of the outer one (i.e. S=o.5). The magnitude of S is selected 0.5, because based on the previous investigations (see e.g. [29]), this value of S results in better crushing responses compared to other values of S (i.e. 0, 0.25, 0.75 and 1). Perimeter of the outer octagonal tube, thickness and length of the tubes are taken 320mm, 2mm and 400mm, respectively. Eight holes with three different shapes of rectangle, hexagon and ellipse are assumed on the both inner and outer walls of the octagonal columns, as seen in Fig. 1. The parameter H, shown in Fig. 1, is assumed to be 50 mm for all the columns with different hole shapes. For simplicity, the holed octagonal columns studied in this paper are labeled as OMCCR, OMCCH and OMCCE, which represents the octagonal multi-cell columns with rectangular, hexagonal and elliptical hole shapes, respectively. Furthermore, OMCC corresponds to the plain octagonal multi-cell column (or octagonal multi-cell column without any hole). Dimensions of the holes are expressed by parameters w and h, as shown in Fig. 1. Different dimensions of holes can be generated on the walls of the octagonal column by changing the values of w and h. Thus, crushing capability of the octagonal multi-cell columns with different hole shapes and dimensions, listed in Table 1, is studied in the present task.

Table 1 The Octagonal multi-cell columns studied in this paper

[DOI: 10.22068/ase.2020.433]

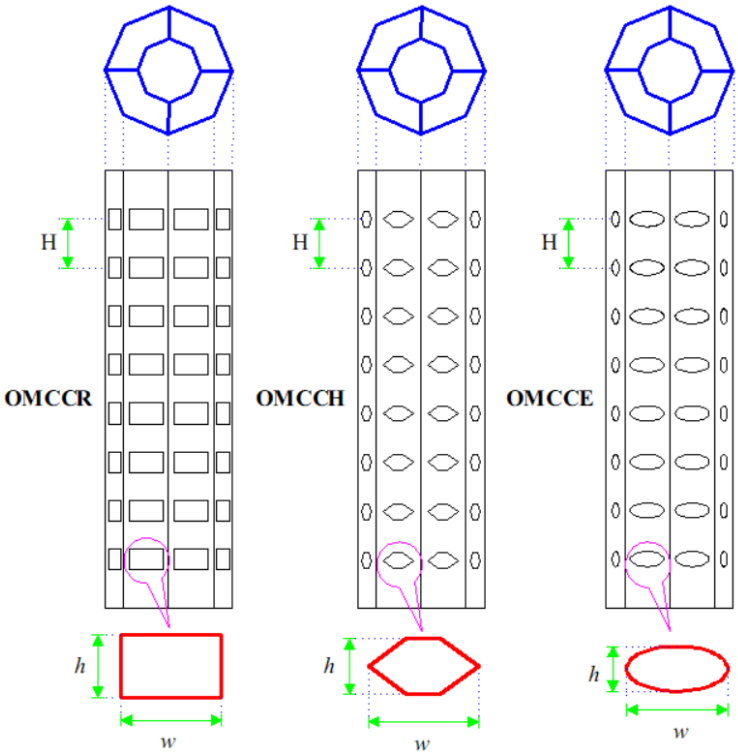

Fig. 1 Geometry of octagonal multi-cell column with rectangular (OMCCR), hexagonal (OMCCH) and elliptical (OMCCE) hole

Table 1 The Octagonal multi-cell columns studied in this paper

Column type	Tag	*w* (mm)	*h* (mm)
Octagonal Multi-cell Column (Plain)	OMCC	0	0
Octagonal Multi-cell Column with rectangular hole	OMCCR (*w*-*h*)	5, 10, 15	5, 10, 15
Octagonal Multi-cell Column with hexagonal hole	OMCCH (*w*-*h*)	6.03, 12.07, 20	6.03, 12.07, 24.14
Octagonal Multi-cell Column with elliptical hole	OMCCE (*w*-*h*)	6.36, 12.73, 20	6.36, 12.73, 25.27

The boundary and impact conditions assumed in this research is such that one end of the columns is fully fixed in all directions, while the other end is kept free (see Fig. 2). A rigid-wall with mass of 600kg and initial velocity of 15m/s vertically impacts upon the free end of the column, and the energy of rigid-wall is supposed to be absorbed by the column. In order to compare the columns studied in this task in terms of crushing capacity, the maximum deformation of the columns is considered 300 mm, which is 75% of the total length of the columns.

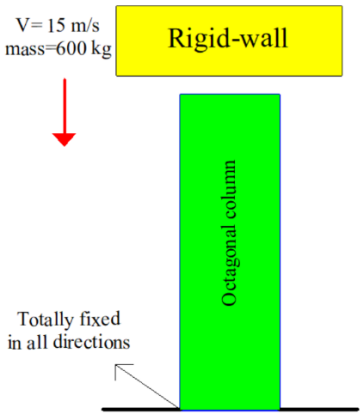

Fig. 2 Boundary and impact conditions

[DOI: 10.22068/ase.2020.433]

Material of the columns is considered aluminum alloy AA6060-T4, and its mechanical properties are as follows: σ_y = 80MPa, σ_{ut} = 173MPa, E = 68.2GPa, ρ = 2700kg/m^3, and υ = 0.33. Meanwhile, the power law exponent is assumed as n=0.23 for this material [30].

Finite element code LS-DYNA is used in this research to model crushing behavior of the multi-cell columns. Shell elements with 4 nodes and five integration points along the thickness are employed to simulate the columns in LS-DYNA. It is pointed out that mesh convergence analysis is carried out in the finite element analyses to gain a suitable element size, i.e. 2.5mm×2.5mm, to correctly extract the crushing parameters. Automatic-Surface to Surface contact algorithm is employed to model the contact between the rigid-wall and columns. Moreover, the contact condition between the column walls during the collapse is also modeled by Automatic-Single-Surface algorithm to avoid interpenetration of the walls. Meanwhile, the friction coefficient in all contacts is regarded as 0.2 [31, 32]. The material of the columns is also modeled by Modified-Piecewise-Linear-Plasticity in the LS-DYNA.

3. Validation of the FE model

For the purpose of ensuring the results of numerical simulations, the finite element model generated in LS-DYNA is validated herein. An experiment is performed on the holed square column illustrated in Fig. 3. The holed square column has a cross-sectional dimensions of 50mm×50mm, length of 100mm and thickness of 2.2mm. Four holes of 10 mm diameter are created on the square column walls, while center-to-center distance of the holes is regarded 23mm. It is pointed out that the material of square column is AA6060-T4, which its mechanical properties have been described above. The experiment is carried out such that the column is put upon the lower fixture of the universal test machine, and the upper fixture is then moved downwards with a displacement rate of 10 mm/min. The force-displacement curve obtained from the experiment is shown in Fig. 3. The mentioned square column is then simulated in LS-DYNA. Collapse modes together with the force-displacement curves obtained from the experiment and numerical simulation are exhibited in Fig. 3. Based on Fig. 3, good agreements are achieved between the numerical and experimental results including the force–displacement curves and the collapse modes, indicating that the finite element simulations are able to suitably predict the crashworthiness behavior of the holed columns. As a result, the numerical analyses in LS-DYNA can model the crushing behavior of octagonal columns with sufficient accuracy.

Square column	Experimental and numerical collapse modes

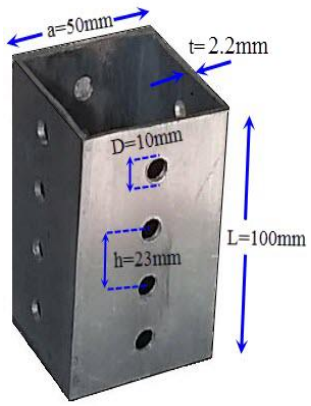

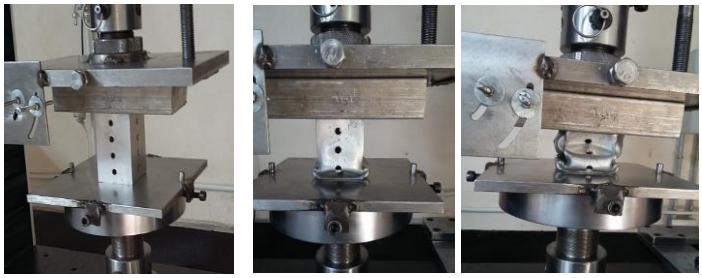

[DOI: 10.22068/ase.2020.433]

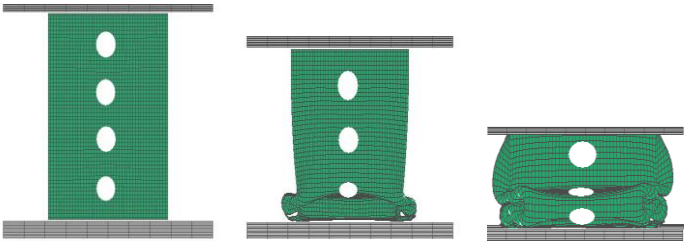

Force-displacement responses

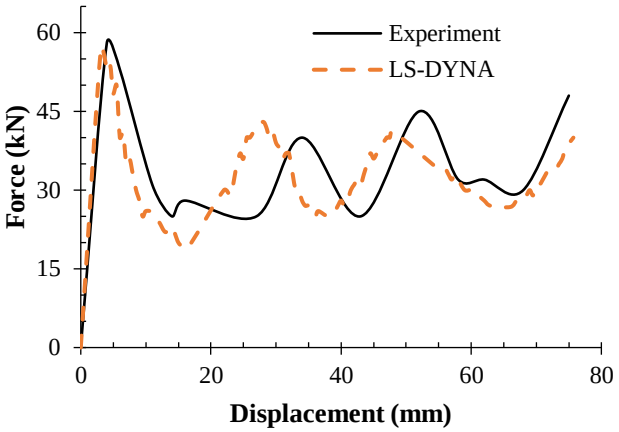

Fig. 3 Experimental and numerical results

In order to further validate the accuracy of finite element model generated in this research, the mean crushing force obtained from the finite element model is compared with that obtained from the simplified super folding element (SSFE) method developed by Chen and Wierzbicki [10]. In the theory proposed by Chen and Wierzbicki [10], a basic element includes three extensional triangular elements and three stationary hinge lines, as illustrated in Fig 4. The mean crushing force of this element with a length of $2H$ is calculated using the energy conservation of the system. Based on the energy balance of the system, the external work done in the compression equals to the plastic deformation in bending and membrane, as follows:

$$2HP_{\mathrm{m}}k = E_{\text{bending}} + E_{\text{membrane}} \tag{1}$$

where, P_{m}, k, E_{bending} and E_{membrane} refer to the mean crushing force, the effective crushing distance coefficient, the bending energy and the membrane energy, respectively. According to literature, the crushing distance coefficient k has a value between 0.7 and 0.75. In this research, the value of k is assumed as 0.73.

[DOI: 10.22068/ase.2020.433]

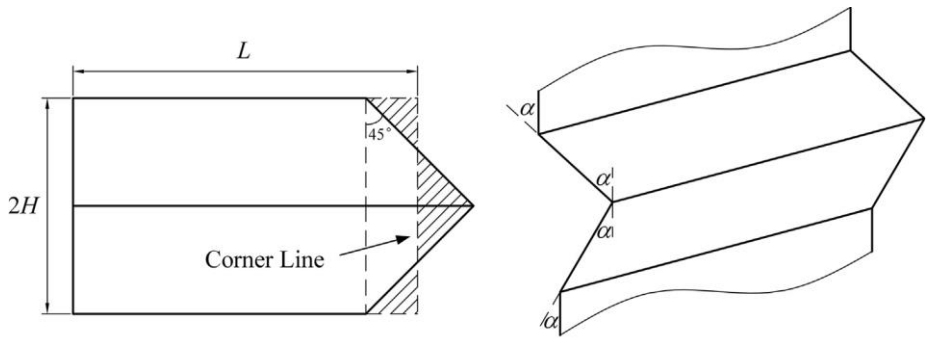

Fig. 4 a) Extensional elements and b) stationary hinge lines [30]

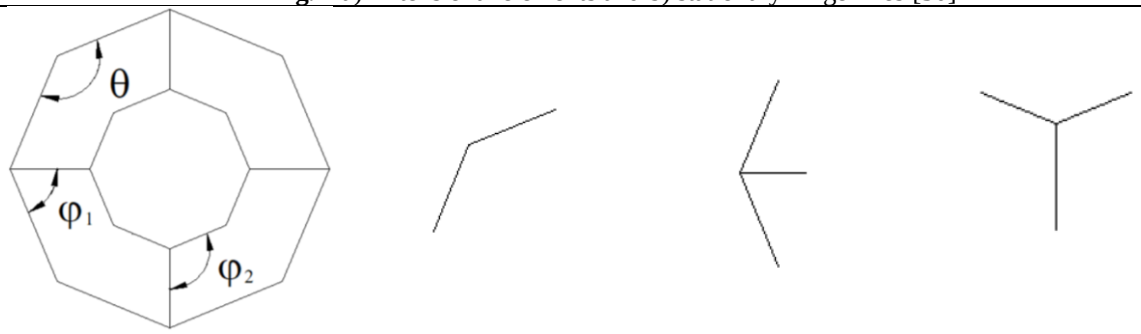

Octagonal tube	Corner element (θ=135°)	3- panel angle element (φ_1=67.5°)	3- panel angle element (φ_2=112.5°)

Fig. 5 Octagonal tube together with the basic elements

The bending energy E_{bending} can be calculated by summation of the energy absorbed at the three stationary hinge lines.

The bending energy E_{bending} can be calculated by summation of the energy absorbed at the three stationary hinge lines.

$$E_{\text{bending}} = \sum_{i=1}^{3} M_0 \alpha_i L_i \quad (2)$$

where, M_0 (*i.e.* moment of fully plastic bending of the flange) equals to $\sigma_0 t^2/4$, α_i expresses the angle of rotation at the hinge line and L_i corresponds to the length of the flange. Furthermore, σ_0 and t are the flow stress of material and wall thickness, respectively. The flow stress σ_0 can be written as follows:

$$\sigma_0 = \sqrt{\frac{\sigma_y \sigma_u}{1+n}} \quad (3)$$

In this equation, the parameters of σ_y, σ_u and n represent the yield stress, ultimate stress and strain hardening exponent, respectively. Meanwhile, their values for the Aluminum alloy used in this research are given in *Section 2*.

According to SSFE theory, the flanges are completely flattened after the axial collapse of 2*H*. Hence, the values of rotation angles are obtained as $\pi/2$, π and $\pi/2$. Accordingly, the bending energy can be simplified to:

$$E_{\text{bending}} = 2\pi M_0 L_c \quad (4)$$

where, L_c is the total length of the flanges.

In order to calculate the membrane energy dissipation subjected to axial loading, the octagonal tube described in *Section* 2 (without any hole) is divided into two types of basic elements including the corner element and 3-panel angle element, as displayed in Fig. 5.

Thus, the theoretical formulas of the membrane energy for these elements are written as:

$$E_{\text{membrane}}^{\text{corner}}(\theta) = \frac{4M_0 H^2 \tan(\theta/2)}{(\tan(\theta/2)+0.05/\tan(\theta/2))t/1.1} \quad (5)$$

[DOI: 10.22068/ase.2020.433]

$$E_{\text{membrane}}^{3-\text{panel}}(\varphi)=\frac{4M_0H^2}{\text{t}}\left(\frac{\tan(\varphi)}{(\tan(\varphi)+0.05/\tan(\varphi))/1.1}+2\tan(\varphi/2)\right) \quad (6)$$

Hence, the total membrane energy can be calculated as below:

$$E_{\text{membrane}}=N_{corner}\,E_{\text{membrane}}^{\text{corner}}(\theta)+N_{3-\text{panel}}\,E_{\text{membrane}}^{3-\text{panel}}(\varphi) \quad (7)$$

where, N_{corner} and $N_{\text{3-panel-I}}$ are the numbers of corner and 3-panel angle elements, respectively. As shown in Fig. 5, the octagonal tube described in *Section* 2 (without any hole) is made up of several corner elements ($\theta = 135°$) and 3-panel angle elements (φ_1=67.5 and φ_2=112.5). Therefore, the membrane energy of the octagonal tube is calculated using the Eqs. (5)-(7) as below:

$$E_{\text{membrane}}^{\text{corner}}(135^{\circ})=\frac{4.363M_0H^2}{\text{t}} \quad (8)$$

$$E_{\text{membrane}}^{3-\text{panel}}(\varphi_1)=\frac{4M_0H^2}{\text{t}}\left(\frac{\tan(67.5^{\circ})}{\tan(67.5^{\circ})+\frac{0.05}{\tan(67.5^{\circ})}/1.1}+2\tan(33.75^{\circ})\right)=9.308\frac{M_0H^2}{t} \quad (9)$$

$$E_{\text{membrane}}^{3-\text{panel}}(\varphi_2)=\frac{4M_0H^2}{\text{t}}\left(\frac{\tan(112.5^{\circ})}{\tan(112.5^{\circ})+\frac{0.05}{\tan(112.5^{\circ})}/1.1}+2\tan(112.5^{\circ})\right)=15.936\frac{M_0H^2}{t} \quad (10)$$

$$E_{\text{membrane}}=4\left(E_{\text{membrane}}^{\text{corner}}(\theta)+E_{\text{membrane}}^{3-\text{panel}}(\varphi_1)+E_{\text{membrane}}^{3-\text{panel}}(\varphi_2)\right)=118.428\frac{M_0H^2}{t} \quad (11)$$

On the other hand, the bending energy for the octagonal tube using the Eq. (4) is written as below:

$$E_{bending}=2\pi M_0L_c=2\pi M_0(1.82P) \quad (12)$$

By substituting the Eqs. (11)-(12) into Eq. (1), we would have:

$$2P_mH.K=2\pi M_0(1.82P)+118.428\frac{M_0H^2}{t}\rightarrow P_m=\frac{1.82\pi M_0P}{H.K}+59.214\frac{M_0H}{Kt} \quad (13)$$

where, P is the perimeter of the outer tube and is set to be 320 mm. It is worth noting that L_c is the total wall length of the tube cross-section, and equals to 1.82P. Based on the stationary condition, the half-wavelength H can be obtained as:

$$\frac{\partial P_m}{\partial H}=0\rightarrow H=\sqrt{0.0965Pt}=0.31P^{\frac{1}{2}}t^{\frac{1}{2}} \quad (14)$$

Substitute Eq. (14) into Eq. (13) to obtain the mean crushing force:

$$P_m=\frac{36.78}{K}M_0P^{\frac{1}{2}}t^{\frac{-1}{2}}\ \&\ M_0=\sigma_0\frac{t^2}{4}\rightarrow P_m=\lambda\frac{9.195}{K}\sigma_0P^{\frac{1}{2}}t^{\frac{3}{2}}\ ;\lambda=1.3\ \&\ k=0.73 \quad (15)$$

where, λ refers to the dynamic factor. When a tube is subjected to dynamic loading, dynamic effects including strain rate effect and inertia effect must be taken account in the calculations. Since the material used in this research (i.e. aluminum) is not sensitive to the strain rate, its effect is neglected. Thus, the dynamic factor λ mainly corresponds to the inertia effect. Based on the previous studies, a value between 1.3 and 1.6 is recommended for the dynamic factor λ. Therefore, the value of λ is assumed to be 1.3 in this research. By placing the values of different parameters for the octagonal tube used in this research into Eq. (15), the value of mean crushing force is calculated as $P_m=87.881\ k$N.

On the other hand, the mean crushing force is obtained as $P_m=\frac{\text{Energy absorbed by octagonal tube}}{Maximum\ rigid-wall\ displacement}=\frac{26.486}{0.300}=88.28\ k$N from the finite element analyses. Compression of the theoretical result and finite element result reveals that there is a good consistency between these results, and the discrepancy of the mean crushing force is less than 0.4%. Therefore, the finite element model is adequately validated, and can be employed for further studies.

[DOI: 10.22068/ase.2020.433]

Table 2 Crushing parameters obtained from the numerical simulations

Octagonal column	*w* (mm)	*h* (mm)	*SEA* (kJ/kg)	F_{max} (kN)
OMCC	0	0	17.52	142.31
OMCCR(5-5)	5	5	16.01	121.34
OMCCR(10-5)	10	5	16.18	111.91
OMCCR(15-5)	15	5	18.09	116.65
OMCCR(5-10)	5	10	19.65	128.05
OMCCR(10-10)	10	10	20.43	113.99
OMCCR(15-10)	15	10	23.95	126.37
OMCCR(5-15)	5	15	20.10	126.55
OMCCR(10-15)	10	15	20.55	111.52
OMCCR(15-15)	15	15	23.18	119.65
OMCCH(6.03-6.03)	6.03	6.03	16.70	123.21
OMCCH(12.07-6.03)	12.07	6.03	16.94	113.70
OMCCH(20-6.03)	20	6.03	19.44	119.46
OMCCH(6.03-12.07)	6.03	12.07	20.02	129.60
OMCCH(12.07-12.07)	12.07	12.07	20.54	119.36
OMCCH(20-12.07)	20	12.07	24.53	127.37
OMCCH(6.03-24.14)	6.03	24.14	20.56	128.56
OMCCH(12.07-24.14)	12.07	24.14	21.64	112.76
OMCCH(20-24.14)	20	24.14	24.81	126.13
OMCCE(6.36-6.36)	6.36	6.36	16.18	126.94
OMCCE(12.73-6.36)	12.73	6.36	16.40	116.10
OMCCE(20-6.36)	20	6.36	19.05	123.08
OMCCE(6.36-12.73)	6.36	12.73	18.62	132.31
OMCCE(12.73-12.73)	12.73	12.73	19.57	122.98
OMCCE(20-12.73)	20	12.73	23.41	129.39
OMCCE(6.36-25.27)	6.36	25.27	19.80	131.50
OMCCE(12.73-25.27)	12.73	25.27	20.66	117.87
OMCCE(20-25.27)	20	25.27	24.30	128.48

4. Numerical results and discussion

There are several crushing parameters to evaluate the columns in terms of crashworthiness capability. Specific energy absorption (*SEA*) is one of the important parameters for indicating crashworthiness performance of thin-walled columns particularly when the weight of columns is not identical. As is well known, the greater *SEA* results in the better column in crashworthiness point of view. This parameter is described as follows:

$$SEA = \frac{\int_0^{\delta_{max}} F(\delta) d\delta}{m} \qquad (16)$$

Displacement of the rigid-wall is regarded by δ, and the maximum rigid-wall displacement is therefore stated by parameter δ_{max}, which is considered 300mm in this investigation. $F(\delta)$ states the crush force variations versus the displacement of the rigid-wall, and *m* is the mass of a column. It is pointed out that the force *F* and displacement δ corresponds to the rigid-wall force (i.e. *rwforce*) and displacement, respectively, which are simply extracted from numerical simulations.

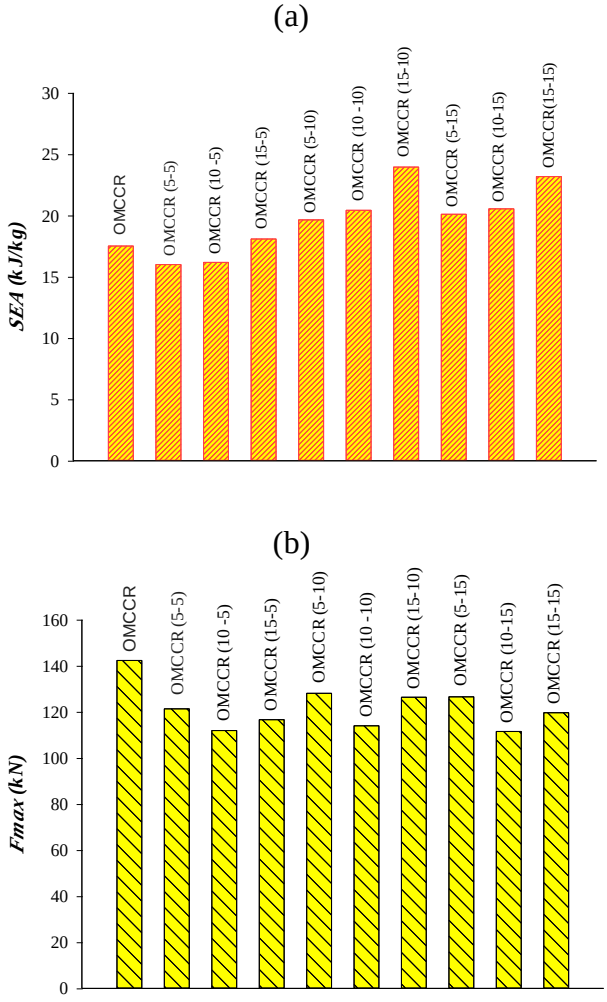

Fig. 6 Crushing parameters, a) *SEA* b) F_{max}, for the octagonal multi-cell columns with rectangular holes

F_{max} is another important parameter for evaluating thin-walled columns, which known as the maximum crush force. This parameter is determined as the maximum force present

[DOI: 10.22068/ase.2020.433]

during the crushing process of a column. The value of F_{max} should be as small as possible to prevent serious damages to passengers during a collision. Hence, the lower F_{max} results in the better column.

Fig. 6 shows the crushing parameters, *SEA* and F_{max}, for the octagonal multi-cell columns with rectangular holes. Based on Fig. 6a, the columns including rectangular holes (i.e. OMCCR) have greater value of *SEA* than the plain octagonal multi-cell column (i.e. OMCC). For the identical value of hole height (or *h*), the value of *SEA* increases with increase in the hole length (or *w*). Furthermore, for the identical value of hole length (or *w*), the value of *SEA* increases with increase in the hole height from *h*=5 mm to 10 mm, and then nearly remains constant (from *h*=10 mm to *h*=15 mm). Thus, among the octagonal columns with rectangular holes with different dimensions, the OMCCR (15-10) exhibits the greatest value of *SEA* i.e. 37% more than that of the plain octagonal column (i.e. OMCC). Fig. 6b shows the values of F_{max} for the octagonal columns with rectangular holes; in which, the holed columns have a lower value of F_{max} compared to the plain octagonal column. Additionally, by increasing the hole length (or *w*), the value of F_{max} initially decreases and then enhances. Thus, the minimum value of F_{max} is achieved for the holed columns with *w*=10 mm.

Fig. 7a shows the values of *SEA* for octagonal columns including hexagonal holes; in which, the effect of dimensions of *w* and *h* on the *SEA* values is identical to the trend achieved for the rectangular holes displayed in Fig. 6a. In other words, the octagonal columns including hexagonal holes (i.e. OMCCH) exhibit better crushing performance than the plain octagonal multi-cell column (i.e. OMCC). For the identical value of *h*, the value of *SEA* enhances with increase in the value of *w*. Moreover, for the identical values of *w*, the value of *SEA* enhances with increase in the value of *h* from 6.03 mm to 12.07 mm, and then nearly remains constant from *h*=12.07 mm to *h*=24.14 mm. Therefore, among the octagonal columns with hexagonal holes with different dimensions, the OMCCH (20-24.14) demonstrates the greatest value of *SEA* i.e. 42% more than that of the plain octagonal column (i.e. OMCC). Fig. 7b plots the values of F_{max} for the octagonal multi-cell columns including hexagonal holes; in which, the holed columns have lower value of F_{max} than the plain octagonal column (i.e. OMCC). Moreover, as the value of *w* enhances, the value of F_{max} initially reduces, and then enhances. Hence, the hexagonal holed columns with *w*=12.07 mm have the lowest value of F_{max}.

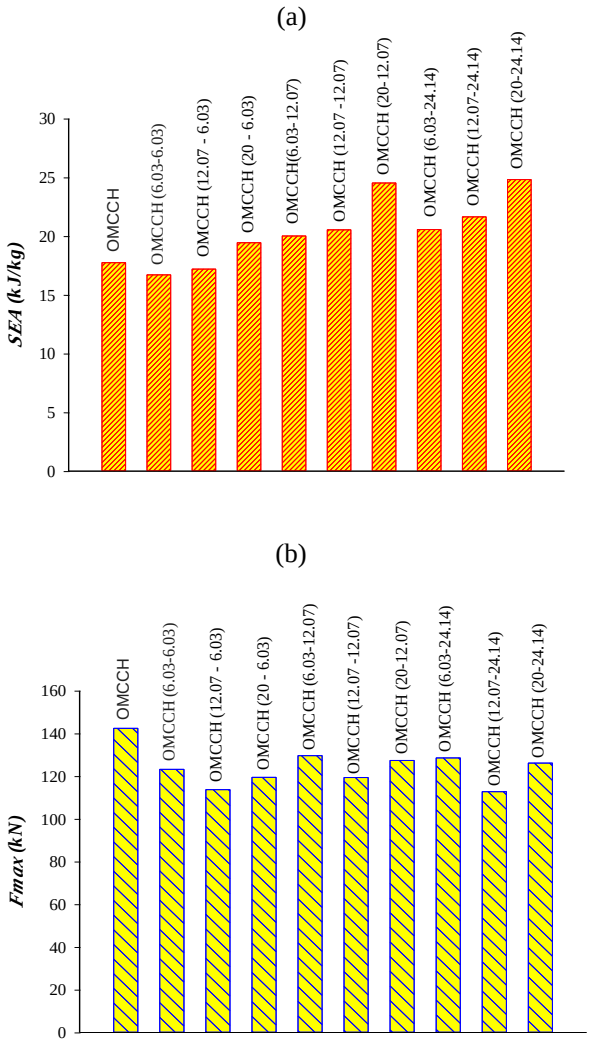

Fig. 7 Crushing parameters, a) *SEA* b) F_{max}, for the octagonal multi-cell columns with hexagonal holes

Fig. 8 displays the results for the octagonal multi-cell columns including elliptical holes. The results of *SEA* and F_{max} for these columns are identical to those observed for the columns with rectangular and hexagonal holes. According to Fig. 8a, the OMCCE (20-25.27) demonstrates the greatest value of *SEA* i.e. 39%

[DOI: 10.22068/ase.2020.433]

higher than that of the plain octagonal column (i.e. OMCC).

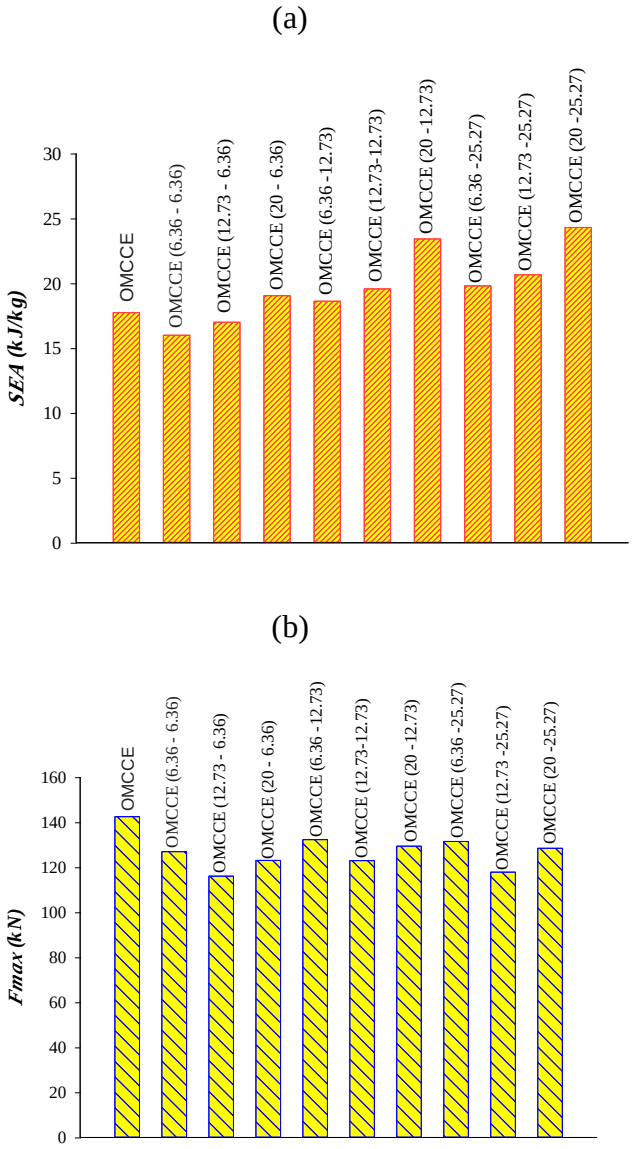

Fig. 8 Crushing parameters, a) *SEA* b) F_{max}, for the octagonal multi-cell columns with elliptical holes

Based on the abovementioned results given for the octagonal columns with different shapes and dimensions of holes, it can be concluded that the hexagonal hole gives the greatest value of *SEA*. In other words, the hexagonal holes present on the octagonal column walls (i.e. OMCCH (20-24.14)) improve crushing capacity by 42% in comparison to the plain octagonal column. On the other hand, the value of F_{max} for the OMCCH is also lower than that for the plain octagonal column (i.e. OMCC). Consequently, a significant improvement in the crushing performance is found by using the technique of generating holes on the column walls.

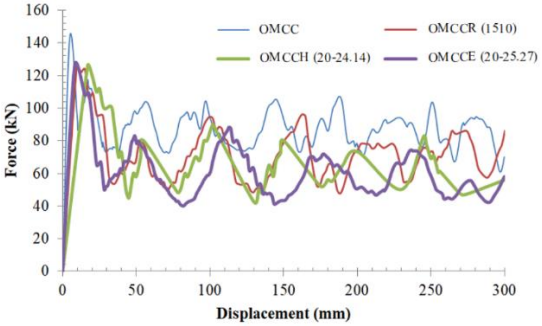

Fig. 9 Force-displacement curves obtained from the numerical simulations for selected octagonal columns

Fig. 9 shows crush force-displacement curves for the selected octagonal columns. As is evident from this figure, the load initially increases to gain a peak value, and then oscillates several times because of progressive wrinkles. It is also pointed out that the plain octagonal column has higher initial peak force than the holed columns, which is dangerous for the passengers during a vehicle collision.

Fig. 10 displays progressive collapsing modes for the selected octagonal columns with different hole shapes. Based on this figure, all the holed columns collapse in diamond mode.

[DOI: 10.22068/ase.2020.433]

Fig. 10 Collapsing mode of selected octagonal columns with different hole shapes

5. Conclusion

In this paper, crushing behavior of octagonal multi-cell columns including three different shapes of holes (i.e. rectangle, hexagon and ellipse) is evaluated. In the first phase of this research, the finite element model generated in LS-DYNA is validated with experimental data. Afterwards, crushing parameters including *SEA* and F_{max} are obtained from the validated model in LS-DYNA. Based on the results, a significant improvement in the crushing capability is observed by generating holes on the column walls. The results show that for the identical value of hole height (or *h*), the value of *SEA* increases with increase in the hole length (or *w*). Furthermore, for the identical value of hole length (or *w*), the value of *SEA* increases with increase in the hole height, and then nearly remains constant.

It is noticed that the OMCCR (15-10), OMCCH (20-24.14) and OMCCE (20-25.27) increases the value of *SEA* by 37%, 42%, and 39%, respectively compared to the plain octagonal column. Meanwhile, all the holed columns demonstrate lower value of F_{max} compared to the plain column. As such, by increasing the hole length (or *w*), the value of F_{max} initially decreases, and then enhances.

References

[1] S. Wu, G. Zheng, G. Sun, Q. Liu, G. Li, Q. Li, On design of multi-cell thin-wall structures for crashworthiness, International Journal of Impact Engineering 88 (2016) 102-117.

[2] X. Zhang, Z. Wen, H. Zhang, Axial crushing and optimal design of square tubes with graded thickness, Thin-Walled Structures 84 (2014) 263-274.

[3] R. Lu, X. Liu, S. Chen, X. Hu, L. Liu, Axial crashing analysis for tailor rolled square tubes with axially graded both wall thickness and material strength, Thin-Walled Structures 117 (2017) 10-24.

[4] W. Abramowicz, N. Jones, Dynamic progressive buckling of circular and square tubes, International Journal of Impact Engineering 4(4) (1986) 243-270.

[5] Z. Liu, Z. Huang, Q. Qin, Experimental and theoretical investigations on lateral crushing of aluminum foam-filled circular tubes, Composite Structures 175 (2017) 19-27.

[6] M. Alkbir, S. Sapuan, A. Nuraini, M.R. Ishak, Effect of geometry on crashworthiness parameters of natural kenaf fibre reinforced composite hexagonal tubes, Materials & Design 60 (2014) 85-93.

[7] S. Hou, Q. Li, S. Long, X. Yang, W. Li, Design optimization of regular hexagonal thin-walled columns with crashworthiness criteria, Finite elements in analysis and design 43(6) (2007) 555-565.

[8] Y. Liu, M. Day, Development of simplified finite element models for straight thin-walled tubes with octagonal cross section, International Journal of Crashworthiness 12(5) (2007) 503-508.

[DOI: 10.22068/ase.2020.433]

[9] P.H. Tehrani, S. Pirmohammad, Study on Crashworthiness Characteristics of Several Concentric Thin Wall Tubes, ASME 2010 10th Biennial Conference on Engineering Systems Design and Analysis, American Society of Mechanical Engineers, 2010, pp. 1-8.
[10] W. Chen, T. Wierzbicki, Relative merits of single-cell, multi-cell and foam-filled thin-walled structures in energy absorption, Thin-Walled Structures 39(4) (2001) 287-306.
[11] X. Zhang, G. Cheng, A comparative study of energy absorption characteristics of foam-filled and multi-cell square columns, International Journal of Impact Engineering 34(11) (2007) 1739-1752.
[12] H.-S. Kim, New extruded multi-cell aluminum profile for maximum crash energy absorption and weight efficiency, Thin-Walled Structures 40(4) (2002) 311-327.
[13] X. Zhang, H. Zhang, Energy absorption of multi-cell stub columns under axial compression, Thin-Walled Structures 68 (2013) 156-163.
[14] X. Zhang, H. Zhang, Axial crushing of circular multi-cell columns, International Journal of Impact Engineering 65 (2014) 110-125.
[15] X. Zhang, G. Cheng, H. Zhang, Theoretical prediction and numerical simulation of multi-cell square thin-walled structures, Thin-Walled Structures 44(11) (2006) 1185-1191.
[16] Q. Chang, D. Fangliang, Y. Shu, W. Dong, Energy-absorbing characteristics of a tapered multi-cell thin-walled tube under ob- lique impact, Journal of Vibration and Shock 31(24) (2012) 102-107.
[17] P. Sadjad, E. Mohammad-Hossein, E.-M. Sobhan, Crashworthiness of double-cell conical tubes with different cross sections subjected to dynamic axial and oblique loads, Journal of Central South University 25(3) (2018) 632-645.
[18] T. Tran, S. Hou, X. Han, W. Tan, N. Nguyen, Theoretical prediction and crashworthiness optimization of multi-cell triangular tubes, Thin-Walled Structures 82 (2014) 183-195.
[19] T. Tran, A. Baroutaji, Crashworthiness optimal design of multi-cell triangular tubes under axial and oblique impact loading, Engineering Failure Analysis 93 (2018) 241-256.
[20] Z. Tang, S. Liu, Z. Zhang, Analysis of energy absorption characteristics of cylindrical multi-cell columns, Thin-Walled Structures 62 (2013) 75-84.
[21] M. Krolak, K. Kowal-Michalska, R. Mania, J. Swiniarski, Experimental tests of stability and load carrying capacity of compressed thin-walled multi-cell columns of triangular cross-section, Thin-Walled Structures 45(10) (2007) 883-887.
[22] W. Hong, H. Fan, Z. Xia, F. Jin, Q. Zhou, D. Fang, Axial crushing behaviors of multi-cell tubes with triangular lattices, International Journal of Impact Engineering 63 (2014) 106-117.
[23] S. Pirmohammad, S.E. Marzdashti, Crushing behavior of new designed multi-cell members subjected to axial and oblique quasi-static loads, Thin-Walled Structures 108 (2016) 291-304.
[24] S. Pirmohammad, S.E. Marzdashti, Crashworthiness optimization of combined straight-tapered tubes using genetic algorithm and neural networks, Thin-Walled Structures 127 (2018) 318-332.
[25] A.A. Nia, M. Parsapour, Comparative analysis of energy absorption capacity of simple and multi-cell thin-walled tubes with triangular, square, hexagonal and octagonal sections, Thin-Walled Structures 74 (2014) 155-165.
[26] S.C.K. Yuen, G. Nurick, R. Starke, The energy absorption characteristics of double-cell tubular profiles, Latin American Journal of Solids and Structures 5(4) (2008) 289-317.
[27] G. Sun, S. Li, Q. Liu, G. Li, Q. Li, Experimental study on crashworthiness of empty/aluminum foam/honeycomb-filled CFRP tubes, Composite Structures 152 (2016) 969-993.
[28] S. Esmaeili-Marzdashti, S. Pirmohammad, S. Esmaeili-Marzdashti, Crashworthiness analysis of s-shaped structures under axial impact loading, Latin American Journal of Solids and Structures 14(5) (2017) 743-764.
[29] S. Pirmohammad, H. Nikkhah, Crashworthiness investigation of bitubal columns reinforced with several inside ribs under axial and oblique impact loads, Proceedings of the Institution of Mechanical Engineers, Part D: Journal of Automobile Engineering (2017) 0954407017702986.

[DOI: 10.22068/ase.2020.433]

[30] L. Zhang, Z. Bai, F. Bai, Crashworthiness design for bio-inspired multi-cell tubes with quadrilateral, hexagonal and octagonal sections, Thin-Walled Structures 122 (2018) 42-51.
[31] J. Fang, Y. Gao, G. Sun, N. Qiu, Q. Li, On design of multi-cell tubes under axial and oblique impact loads, Thin-Walled Structures 95 (2015) 115-126.
[32] Z. Zhang, S. Liu, Z. Tang, Crashworthiness investigation of kagome honeycomb sandwich cylindrical column under axial crushing loads, Thin-Walled Structures 48(1) (2010) 9-18.

[DOI: 10.22068/ase.2020.433]